Current Biology

A skeleton from the Middle Jurassic of Scotland illuminates an earlier origin of large pterosaurs

Graphical abstract

A **skeleton** from the **Middle Jurassic** of **Scotland** illuminates an earlier origin of **large** pterosaurs

Estimated wingspan >2.5 meters, largest of any well preserved Jurassic pterosaurs

Dearc sgiathanach sp. nov
jark ski-an-ach

Etymology Scottish Gaelic, for 'winged reptile' and 'reptile from Skye'

Research authors:
Natalia Jagielska, Michael O'Sullivan. Gregory F. Funston, Ian B. Butler, Thomas J. Challands, Neil D. L. Clark, Nicholas C. Fraser, Amelia Penny, Dugald A. Ross, Mark Wilkinson & Stephen L. Brusatte

Bone histology shows the individual was still actively growing when it died, and would have been larger as an adult

It anchors a clade of large **Jurassic pterosaurs** that evolved wide **wingspans** before the Cretaceous

Dearc

Angustinaripterus

Authors

Natalia Jagielska, Michael O'Sullivan, Gregory F. Funston, ..., Dugald A. Ross, Mark Wilkinson, Stephen L. Brusatte

Correspondence

n.jagielska@sms.ed.ac.uk (N.J.),
stephen.brusatte@ed.ac.uk (S.L.B.)

In brief

Jagielska et al. report a fossil pterosaur skeleton from the Middle Jurassic (ca. 167 million years ago) of Scotland, belonging to a new genus and species, *Dearc sgiathanach*. With a wingspan of over 2.5 m, it was the size of the largest modern-day flying birds and shows that pterosaurs developed to a large size earlier than previously thought.

Highlights

- A new pterosaur genus and species from the Middle Jurassic of Scotland is described

- It is represented by a well-preserved fossil skeleton, including the brain endocast

- It was not fully grown when it died and would have had a wingspan of >2.5 m

- Pterosaurs evolved to a considerably larger size earlier than previously recognized

CellPress

Current Biology

CellPress

Report

A skeleton from the Middle Jurassic of Scotland illuminates an earlier origin of large pterosaurs

Natalia Jagielska,[1,7,*] Michael O'Sullivan,[2] Gregory F. Funston,[1] Ian B. Butler,[1] Thomas J. Challands,[1] Neil D.L. Clark,[3] Nicholas C. Fraser,[1,4] Amelia Penny,[1,5] Dugald A. Ross,[6] Mark Wilkinson,[1] and Stephen L. Brusatte[1,4,8,9,*]

[1]School of GeoSciences, University of Edinburgh, Grant Institute, James Hutton Road, Edinburgh, Scotland EH9 3FE, UK
[2]Gortroe Rathkeale, Co Limerick, Ireland
[3]The Hunterian, University of Glasgow, University Avenue, Glasgow, Scotland G12 8QQ, UK
[4]National Museums Scotland, Chambers Street, Edinburgh, Scotland EH1 1JF, UK
[5]School of Biology, University of St Andrews, Biomedical Sciences Research Complex, St. Andrews, Scotland KY16 9ST, UK
[6]Staffin Museum, 6 Ellishadder, Staffin, Isle of Skye, Scotland IV51 9JE, UK
[7]Twitter: @wrycritic
[8]Twitter: @SteveBrusatte
[9]Lead contact
*Correspondence: n.jagielska@sms.ed.ac.uk (N.J.), stephen.brusatte@ed.ac.uk (S.L.B.)
https://doi.org/10.1016/j.cub.2022.01.073

SUMMARY

Pterosaurs were the first vertebrates to evolve flight[1,2] and include the largest flying animals in Earth history.[3,4] While some of the last-surviving species were the size of airplanes, pterosaurs were long thought to be restricted to small body sizes (wingspans ca. <1.8–1.6 m) from their Triassic origins through the Jurassic, before increasing in size when derived long-skulled and short-tailed pterodactyloids lived alongside a diversity of birds in the Cretaceous.[5] We report a new spectacularly preserved three-dimensional skeleton from the Middle Jurassic of Scotland, which we assign to a new genus and species: *Dearc sgiathanach* gen. et sp. nov. Its wingspan is estimated at >2.5 m, and bone histology shows it was a juvenile-subadult still actively growing when it died, making it the largest known Jurassic pterosaur represented by a well-preserved skeleton. A review of fragmentary specimens from the Middle Jurassic of England demonstrates that a diversity of pterosaurs was capable of reaching larger sizes at this time but have hitherto been concealed by a poor fossil record. Phylogenetic analysis places *D. sgiathanach* in a clade of basal long-tailed non-monofenestratan pterosaurs, in a subclade of larger-bodied species (Angustinaripterini) with elongate skulls convergent in some aspects with pterodactyloids.[6] Far from a static prologue to the Cretaceous, the Middle Jurassic was a key interval in pterosaur evolution, in which some non-pterodactyloids diversified and experimented with larger sizes, concurrent with or perhaps earlier than the origin of birds.

RESULTS AND DISCUSSION

Pterosauria Owen, 1842
  Breviquartossa Unwin, 2003
  Rhamphorhynchidae Seeley, 1870
  Rhamphorhynchinae Seeley, 1870
  Angustinaripterini He, 1983

Included species

Angustinaripterus longicephalus, *Sericipterus wucaiwanensis*, and *Dearc sgiathanach* (below).

Diagnosis

Group of rhamphorhynchine pterosaurs sharing a low and elongate skull (height-to-length ratio < 0.2); large antorbital fenestra (20%–35% skull length and >80% orbit dorsoventral height); lacrimal process of jugal nearly perpendicular inclined (90°–110°) to jugal body; strongly inclined quadrate (130°–140° relative to maxilla long axis); cervical vertebrae with considerable change in length-to-width ratio across the neck (1.8 to 1.2, from anterior to posterior); humeral diaphysis slender with muscle scar tubercle.

  Dearc n. gen.
  Type species
  Dearc sgiathanach sp. nov.

Etymology

Scottish Gaelic, with the double meaning of "winged reptile" and "reptile from Skye," paying homage to pterosaurs (winged reptiles) and the Gaelic name for Skye (An t-Eilean Sgitheanach, the "winged isle"). Phonetic pronunciation: jark ski-an-ach.

Holotype

NMS (National Museums Scotland, Edinburgh) G.2021.6.1-4 (Figures 1, 2, 3, S2, and S3), a three-dimensionally preserved articulated skeleton, lacking anterior and dorsal portions of the cranium, left manus, portions of the wings, hindlimb elements, and the distal tail. The fossil was separated into four slabs during
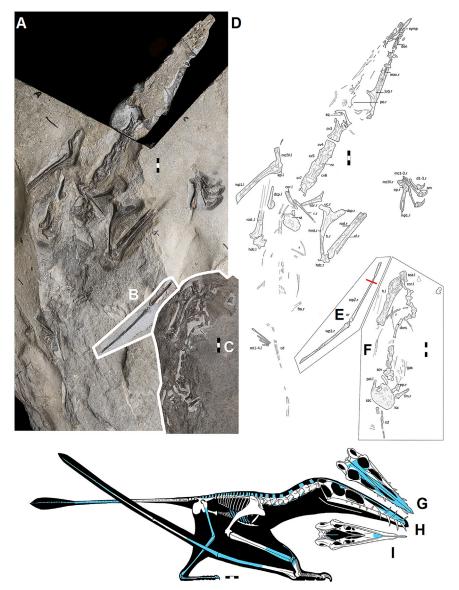
Figure 1. The new Middle Jurassic ptero-saur *Dearc sgiathanach*

(A–C) Photographs of main slab (NMS G.2021.6.1–2), bones in dorsal view (A); wing phalanges 2–3 (NMS G.2021.6.3–4), in dorsal view (B); and main counterslab (NMS G.2021.6.3), bones in ventral view (C).

(D–F) Schematic drawings of (A)–(C).

(G–H) Reconstruction of skull in dorsal (G) and ventral (I) views and skeleton in lateral view (H).

ar, articular region; cd, caudal vertebrae; cor, coracoid; cv, cervical vertebrae; d, digit; den, dentary; dors, dorsal vertebrae; dpc, deltopectoral crest; ep, extensor process; fm, femur; gas, gastralia; hdc, humeral distal condyle; hmt, humeral tubercle; isc, ischium; ju, jugal; max, maxilla; mc, metacarpal; mt, metatarsal; po, postorbital; r, ribs; sac, sacral plate; sca, scapula; scv, sacral (?) vertebrae; sm, sesamoid; sq, squamosal; st, sternum; symp, symphysis; uc, ulnar crest; ul, ulna; wp, wing phalanx; r/l, right/left. Blue on reconstructions are missing regions; red line in (E) is location of histological sectioning. Scale bars, 30 mm.

See Figures S2 and S3.

Diagnosis

Dearc sgiathanach is a rhamphorhynchine pterosaur with the following autapomorphies: tri-tubular vomers with "trident-shaped" precapillary contact, pre-choana depression on the palatal surface of the maxilla, enlarged optic lobes expanded anteroposteriorly, and fourth metatarsal more robust (diameter 2.5×) than mt1-3. For additional information, see STAR Methods.

Bone histology and maturity

Using Bennett's[12] osteologically based ontogenetic stages for the closely related *Rhamphorhynchus*, NMS G.2021.6.1–4 has features of terminal-stage adults, such as large and recurved premaxillary teeth, fused scapula-coracoid, well-developed humeral crests, smooth bone texture, and fused long bone epiphyses. However, some osteological features are indicative of immaturity according to Bennett:[12] portions of the skull are unfused, such as the jugal with the lacrimal, and there appears to be limited fusion in the sacral vertebrae.

Immaturity is corroborated by bone histology (STAR Methods; Data S2). The cortex of a sampled wing phalanx is composed entirely of primary fibrolamellar bone[13] and preserves two prominent lines of arrested growth (LAGs), which indicate that the individual was at least 2 years old at death.[14] The position of the second LAG close to the external bone surface suggests that the individual died shortly after emerging from an annual growth hiatus. The cortex is densely vascularized and has a high proportion of woven bone, indicating a rapid rate of growth throughout life.[15] The presence of vasculature extending to the external bone surface and the absence of an external fundamental

preparation: the main slab contains the majority of bones, exposed in dorsal view (NMS G.2021.6.1), and the main counter slab contains bones exposed ventrally (NMS G.2021.6.3). An additional block contains a wing phalanx (NMS G.2021.6.4). The skull and anterior cervical vertebrae (NMS G.2021.6.2) were separated from the main slab for X-ray computed microtomography (μCT) (Figure 2). Measurements in Data S1A.

Locality and horizon

The specimen was discovered by A.P. in 2017 at Rubha nam Brathairean (Brothers' Point), Trotternish, Isle of Skye, Scotland, in the Lonfearn Member of the Lealt Shale Formation (Bathonian, Middle Jurassic)[9,10] (Figure S1). The skeleton was embedded in a well-sorted lagoonal bioclastic limestone (rich in *Neomiodon*, ostracods, and conchostracans), which overlies and infills dinosaur trackways impressed in subaerially exposed mudstones.[11] These units formed in a marginal marine/nearshore environment that fluctuated between submerged and exposed.

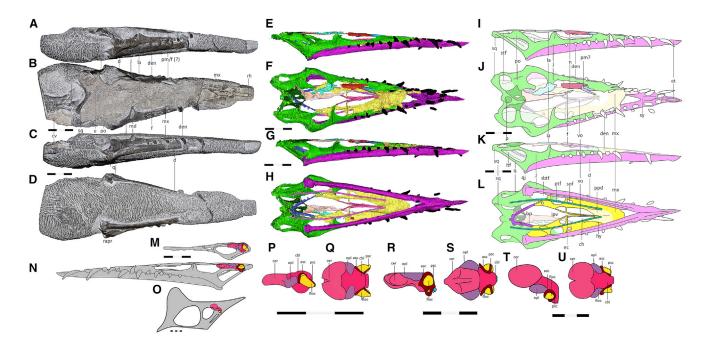⇆ **CellPress**

Figure 2. Skull of the new Middle Jurassic pterosaur *Dearc sgiathanach* and comparisons of pterosaur brain and ear endocasts

(A–L) Photographs (A–D), segmented μCT scan renderings (E–H), and schematic drawings (I–L) of the skull (NMS G.2021.6.2) in, from top to bottom, left lateral (reversed), dorsal, right lateral, and ventral views.

(M–U) Brain and inner ear endocasts of *Rhamphorhynchus* (based on Witmer et al.[7]) (M, P, and Q), *Dearc* (N, R, and S), and *Tapejara* (based on Eck et al.[8]) (O, T, and U), shown in the skull in left lateral view and isolated in left lateral and dorsal views, respectively.

asc, anterior semi-circular canal; bp, basisphenoid; cbl, cerebellum; cer, cerebrum; ch, choana; chl, channels; cv, third cervical; d, dentary; den, dentition; e, endocast; ec, ectopterygoid; et, edentulous anterior tip; f, frontal (?); hy, hyoid; ipv, interpterygoid vacuity; itf, inferior temporal fenestra; j, jugal; la, lacrimal; md, matrix infilled dent; mx, maxilla; n, nasal; olf, olfactory bulb; opl, optic lobe; p, parietal; pm, premaxilla; po, postorbital; ppd, post-palatal depression; psc, posterior semi-circular canal; ptf, pneumatic foramen; q, quadrate; qj, quadratojugal; rapr, retroarticular process; rh, probable placement of rhamphotheca; sof, suborbital fenestra; sq, squamosal; sbtf, subtemporal fenestra; stf, superior temporal fenestra. In (E)–(L), bones that cannot be distinguished in the μCT scan due to fusion or insufficient resolution are conservatively rendered together in one color. Scale bars, 30 mm.
See Figure S2.

---

system indicate that the individual was actively growing when it died. In many respects, the bone microstructure is similar to small, young individuals (<30% adult wingspan; size class I[12]) of *Rhamphorhynchus*[16] and other actively growing juvenile pterosaurs,[17,18] indicating that it is best interpreted as a juvenile or subadult[19] that had not reached adult body size when it perished.

Wingspan and body size

Wingspan—defined as double the summed lengths of the bones of a single wing[5]—is tightly correlated to body mass and wing area in pterosaurs and thus a robust body size proxy.[20] A complete wingspan cannot be measured directly from NMS G.2021.6.1–4 because some wing phalanges are missing. To estimate wingspan, we compiled measurements of complete wingspans of two non-monofenestratans represented by large sample sizes—*Rhamphorhynchus* and *Dorygnathus*—and regressed these against the lengths of individual bones to create predictor formulas (STAR Methods; Data S1C–S1Q). Using *Rhamphorhynchus* scaling, the humerus length (112 mm) and skull length (222 mm) of NMS G.2021.6.1–4 indicate wingspans of 3.8 and 2.2 m, respectively. The largest known *Rhamphorhynchus* (Natural History Museum UK 37002) is considerably smaller, with a wingspan of 1.8 m, humeral length of 79 mm, and skull length

of 202 mm. Using *Dorygnathus* scaling, the humeral length of NMS G.2021.6.1–4 indicates a wingspan of 1.9 m, approximately 10% larger than the largest *Dorygnathus* (1.69 m wingspan, 84 mm humerus).

These results demonstrate that *Dearc* is the largest Jurassic pterosaur yet known, consistent with the fact that its humerus and skull are the longest of any Jurassic specimens. Furthermore, we interpret these results as evidence that *Dearc* likely achieved wingspans over 2.5 m, and perhaps larger (>3 m). This is based on two lines of reasoning. First, we consider the *Rhamphorhynchus* equations, which give larger wingspan estimates, as the most valid predictors: *Rhamphorhynchus* is a closer relative of *Dearc* than is *Dorygnathus*, is known from a larger sample size (and thus generates a regression with tighter error bars and a higher r[2] value), and has a well-established and nearly isometric growth trajectory that makes predicting wingspan from isolated skeletal elements more justifiable.[21] Second, the holotype of *Dearc* (NMS G.2021.6.1–4) was an actively growing juvenile-subadult at death and would have been larger as an adult (STAR Methods).

Description

A detailed description is provided in Data S2, with salient features summarized here. *Dearc* generally conforms to the classic

Figure 3. Postcranial skeleton and dentition of the new Middle Jurassic pterosaur *Dearc sgiathanach*

Photographs of the right manus (A), cervical series (B), pubic region (C), right humerus (D), left humerus (E), left metacarpal-phalanx articular region (F), right maxilla (G), and left pes (H) of NMS G.2021.6.1–4.

ac, anterior caudal vertebrae; ar, articular region; c, condyle; cdv, caudal vertebrae; cor, coracoid; cv, cervical vertebrae; d, dentary; dc, distal condyle; dpc, deltopectoral crest; dvrt, dorsal vertebrae; en, enamel; exp, extensor process; fem, femur; ft, flexor tubercle; gas, gastralia; h, humerus; ic, intercondylar groove; isc, ischium; max, maxilla; md, maxillary dentition; mg, medial groove; mt, metatarsal; nss, neural spine scar; pa, preacetabular process; poz, postzygapophysis ppb, prepubis; prez, prezygapophysis; rad, radius; rb, rib; sac, sacrum; sm, sesamoid; uc, ulnar crest; ul, ulna; un, ungual; vert, vertebra; wp1, wing phalanx one. Scale, 10 mm per bar.

See Figures S2 and S3.

non-monofenestratan body plan, as it has an elongate mandibular symphysis (>20% mandible length), cervical ribs (visible in µCT data of anterior cervicals), a neck shorter than the combined dorsal and sacral series, a short metacarpus (<80% humerus length), and an elongate tail comprised of elongate caudal vertebrae supported by interlocking zygapophyses (Figures 1, 2, and 3). It does, however, possess some features typical of pterodactyloids and often considered part of a "module" unique to their bauplan,[6] including a skull that is longer than the combined dorsal and sacral series and a highly inclined quadrate (Figure 2). Furthermore, although the cervical vertebrae are short and squat as in non-monofenestratans, they are proportionally more elongate than most members of that grade, beginning to approach the proportions of more derived pterosaurs like *Wukongopterus lii* and *Douzhanopterus zhengi*[22,23] (STAR Methods). There is a continuum between two distinct types of dentition: elongate fangs at the snout tip and conical pegs along much of the jaw length (Figures 2 and 3).
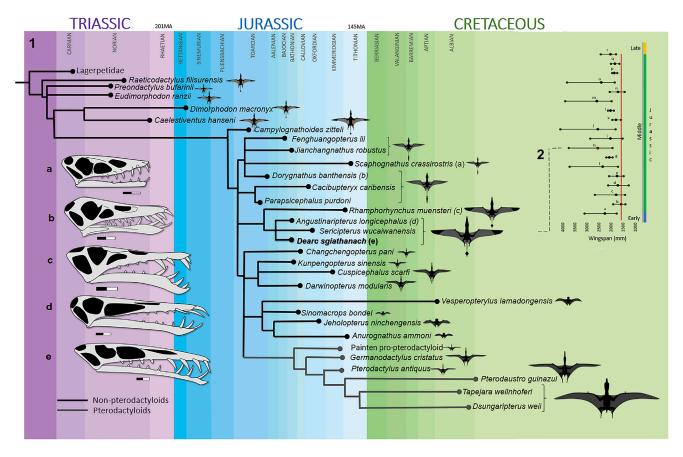
Figure 4. Phylogenetic relationships of the Middle Jurassic pterosaur *Dearc sgiathanach* and wingspan estimates for Jurassic pterosaurs
Strict consensus of most parsimonious trees from phylogenetic analysis, with silhouettes scaled to wingspan (*Dearc* = ca. 2.0 m) (1), and skull reconstructions of key taxa: (A) *Scaphognathus crassirostris* (based on GPIB 1304), (B) *Dorygnathus banthensis* (based on SMNS 55886), (C) *Rhamphorhynchus muensteri* (based on NHMUK R 37002), (D) *Angustinaripterus longicephalus* (based on ZDM T8001), and (E) *Dearc sgiathanach*. Wingspan plot (2): estimated wingspan range for isolated pterosaur remains from the Taynton Limestone collection. See Data S1D for complete element list. (A) NHMUK PV R 36634, (B) GSM 113726, (C) OUM J28352, (D) NHMUK PV R 38016, (E) NHMUK PV R1362, (F) LL12158, (G) NHMUK PV R 40126, (H) NMS G.2021.6.1-4 (*Dearc*), (I) OUM J23046, (J) OUM J28273, (K) NHM UK PV R 40126 B, (L) OUM J28319, (M) OUM J28307, (N) OUM J28271, (O) OUM J28354, (P) LL12160, (Q) OUM J23047, and (R) MJM L K1995. See Figure S4 and Data S1 and S2.

μCT data provide a stellar view of a complete, articulated palate and hyoid of a non-monofenestratan pterosaur in dorsal and ventral view (Figure 2). The heart-shaped choana is cut medially by forking vomers, comprised of three cylindrical rods that converge anteriorly in a trident-shaped contact. There is a thin extension of the ectopterygoid, which rotates around its own axis, forming an elevated ventral border of the postpalatine fenestra, joining the vomers at a perpendicular angle. This "contorted" morphology has not been described in other pterosaurs.

μCT data also provide one of the few brain and inner ear endocasts of a basal pterosaur (Figure 2). Like *Rhamphorhynchus*,[7] *Dearc* had a large cerebrum with optic lobes positioned at the same level as the forebrain and a large flocculus, around which thin and arched semicircular canals looped, that nonetheless did not project to the same lateral level as the cerebrum. In pterodactyloids, however, the brain is highly flexed so that the cerebrum is elevated relative to the optic lobes, and the flocculus is expanded beyond the cerebrum laterally.[7,8,24] In *Dearc*, the optic lobes are larger, anteroposteriorly

longer, and more widely exposed dorsally than in any known basal pterosaur or pterodactyloid (*Rhamphorhynchus*,[7] *Allkauren*,[24] and *Tapejara*[8]).

Phylogenetic analysis

Our phylogenetic analysis focuses on non-monofenestratan pterosaurs and combines data from several independent published analyses[22,25–35] with new characters, while excluding taxa known only from highly immature specimens and characters that exhibit strong ontogenetic variation, resulting in a dataset of 58 taxa scored for 155 characters (Data S1B and S2). *Dearc sgiathanach* is recovered within a large grade of non-monofenestratans, including subclades centered on *Rhamphorhynchus* and *Scaphognathus* (Figure 4). *Dearc* is in the former subclade, where it groups with the Chinese *Angustinaripterus* and *Sericipterus*, in the clade Angustinaripterini, diagnosed here for the first time by several features including a large antorbital fenestra, reclined quadrate, and proportionally elongate anterior cervicals (see above).

Remarks

The holotype of *Dearc sgiathanach* is a rare three-dimensionally preserved pterosaur from the Jurassic, which gives unique insight into the osteology, size, growth, and neuroanatomy of a basal non-monofenestratan. Its most remarkable attribute is its size: its wingspan was ca. 1.9–3.8 m, roughly the size of the largest flying birds today (e.g., wandering albatross), and it was not fully grown at death. Triassic and Jurassic pterosaurs have long been stereotyped as relatively small animals, constrained to wingspans of approximately 1.6–1.8 m or less over the first ca. 70 million years of their evolutionary history,[5] before becoming larger in the latest Jurassic or Early Cretaceous, culminating in airplane-sized giants like *Quetzalcoatlus* with 10-m wingspans.[5] A few tantalizing specimens have hinted at larger Jurassic pterosaurs,[36–38] but these are often limited to one or a few bones, which make body size estimations difficult. *Dearc* is the first Jurassic pterosaur whose wingspan can confidently be estimated at ca. 2.5 m or greater, based on a well-preserved, articulated skeleton.[5] Its closest relatives, *Angustinaripterus* and *Sericipterus*, are also sizeable for Jurassic species, with wingspans previously estimated at 1.6[1]–1.7[38] m extrapolated from patchy fossils. Our regression equations indicate larger wingspans for these taxa: ca. 2–3 m, which is still approximately 10% smaller than *Dearc*. *Dearc*, therefore, anchors a clade of large, long-snouted Jurassic non-monofenestratans: Angustinaripterini.[38]

The large size of *Dearc* prompted us to re-examine fragmentary specimens from the Taynton Limestone,[39] an English unit that formed at the same general time as the Scottish Middle Jurassic deposits, in or along the margins of the same seaway. We identified 17 specimens—all single bones—that yield wingspan estimates of over 1.7 m based on our predictor formulas (above), including several that may have had wingspans of over 3.0 m. The discovery of *Dearc*, and our survey of Taynton specimens, reveals that Jurassic pterosaurs were capable of achieving considerably larger sizes than previously thought. Jurassic pterosaurs may still have been constrained in size—and certainly there is no evidence they approached the grandeur of giant Cretaceous pterodactyloids—but if so, that constraint was at a substantially greater wingspan than 1.6–1.8 m.[5]

Trends in pterosaur size evolution, particularly the shift to increasingly larger species in the Cretaceous, have been interpreted in terms of two main hypotheses, which are not mutually exclusive: (1) advances in the pterodactyloid body plan allowed them to become larger and more efficient fliers than non-pterodactyloids, and (2) the diversification of birds (Avialae) may have driven latest Jurassic/Cretaceous pterosaurs into ever-larger size niches.[5] Our identification of *Dearc* demonstrates that non-pterodactyloids were able to grow to larger sizes by the Middle Jurassic, with some evidence for large pterosaurs back to the Early Jurassic,[37] tens of millions of years before birds underwent their adaptive Cretaceous radiation.[40,41] These size increases seemingly occurred too early for avialans, which are first definitively known from the Late Jurassic, to have been a direct cause. Alternatively, if there was pressure on pterosaurs to become larger, it may have started deep in the Jurassic and involved competition with unrecognized early avialans or other animals,[40] like non-avialan feathered dinosaurs or other pterosaurs.

Not only is *Dearc* large, but it and its closest angustinaripterin relatives possess derived characters considered keystones of the pterodactyloid skull "module," notably an elongate skull and inclined quadrate. Previous work has argued that the transition between non-pterodactyloids and pterodactyloids involved a nearly perfect modular shift, in which features of the skull changed together in a tightly integrated unit, followed by the body, limbs, and tail.[6] While we do not dispute the overarching modularity of the pterosaur skeleton, *Dearc* hints that some of the trademark "pterodactyloid" features convergently evolved in other groups,[42] perhaps due to feeding ecology or other factors. Yet the endocranial anatomy of *Dearc* is distinctly primitive, as it has the unflexed brain and smaller flocculus of basal pterosaurs[7,24] and not the transformed brain of pterodactyloids. Thus, it seems, non-pterodactyloids had a similar neuroanatomy regardless of body size.

Our recognition of large Middle Jurassic pterosaurs exposes a taphonomic bias, to add to the already notoriously problematic record of pterosaurs.[43,44] There were fairly large pterosaurs in the Jurassic (wingspans > 1.8 m), but reasonably complete adult or near-mature skeletons are mostly lacking, for reasons unclear and worthy of further study. The Middle Jurassic age of *Dearc* adds to increasing evidence that this interval—once a frustrating gap in the pterosaur record—was in fact a dynamic time of diversification, in which a variety of basal taxa and early monofenestratan lineages[6,39] coexisted and occupied a range of environments, from open marine to lagoonal, nearshore to desert, around the world. We can now add larger taxa, with derived pterodactyloid-type skull characters, to that roster. As with dinosaurs[45] and mammals,[46] the Middle Jurassic was likely a vibrant time in pterosaur history, not a static and archaic prelude to a Cretaceous explosion of larger,[5] more disparate,[47] more efficient fliers.[20] With the dawn of the Cretaceous, however, the diverse non-monofenestratans disappeared, including larger ones with pterodactyloid convergences. This mystery remains to be solved.

STAR★METHODS

Detailed methods are provided in the online version of this paper and include the following:

- KEY RESOURCES TABLE
- RESOURCE AVAILABILITY
  - Lead contact
  - Materials availability
  - Data and code availability
- EXPERIMENTAL MODEL AND SUBJECT DETAILS
- METHOD DETAILS
  - Fossil genuineness
  - Fossil examination
  - Computed tomography scanning
  - Bone histology
  - Wingspan estimates
  - Stratigraphy, dating, and taphonomy
  - Nomenclatural acts
  - Phylogenetic analysis
  - Institutional abbreviations
- QUANTIFICATION AND STATISTICAL ANALYSIS

Current Biology
Report

CellPress

AUTHOR CONTRIBUTIONS

N.J. led the study of the specimen as part of her PhD project at the University of Edinburgh and performed the descriptive and comparative analysis, assembled the character dataset and conducted the phylogenetic analysis, conducted μCT scan segmentation, drafted all figures (outlines, cladogram, reconstructions, and skeleton models), and edited the text. M.O.S. provided supervision, advice on pterosaur anatomy, wingspan calculations (including the wingspan figure in Figure 4), and assistance with the phylogenetic analysis. S.L.B. supervised N.J.'s PhD project on this specimen, led the field team that collected the specimen, drafted the text of the manuscript, and performed the wingspan statistical analyses. I.B.B. μCT scanned the specimen. G.F.F. conducted the bone histology analysis and photographed the specimen. A.P. discovered the specimen. D.A.R., S.L.B., T.J.C., N.D.L.C., and A.P. collected the specimen. N.D.L.C., N.C.F., and M.W. provided co-supervision. All authors edited and approved the text.

REFERENCES

1. Wellnhofer, P. (1991). The Illustrated Encyclopedia of Pterosaurs (Salamander Books).

2. Witton, M.P. (2013). Pterosaurs: Natural History, Evolution, Anatomy (Princeton University Press).

3. Lawson, D.A. (1975). Pterosaur from the latest cretaceous of west Texas: discovery of the largest flying creature. Science *187*, 947–948.

4. Henderson, D.M. (2010). Pterosaur body mass estimates from three-dimensional mathematical slicing. J. Vertebr. Paleontol. *30*, 768–785.

5. Benson, R.B.J., Frigot, R.A., Goswami, A., Andres, B., and Butler, R.J. (2014). Competition and constraint drove Cope's rule in the evolution of giant flying reptiles. Nat. Commun. *5*, 3567.

6. Lü, J., Unwin, D.M., Jin, X., Liu, Y., and Ji, Q. (2010). Evidence for modular evolution in a long-tailed pterosaur with a pterodactyloid skull. Proc. Biol. Sci. *277*, 383–389.

7. Witmer, L.M., Chatterjee, S., Franzosa, J., and Rowe, T. (2003). Neuroanatomy of flying reptiles and implications for flight, posture and behaviour. Nature *425*, 950–953.

8. Eck, K.E., Elgin, R.A., and Frey, E. (2011). On the osteology of *Tapejara wellnhoferi* Kellner 1989 and the first occurrence of a multiple specimen assemblage from the Santana Formation, Araripe Basin, NE-Brazil. Swiss J. Palaeontol. *130*, 277.

9. Hudson, J.D., and Wakefield, M.I. (2018). The Lonfearn Member, Lealt Shale Formation (Middle Jurassic) of the Inner Hebrides, Scotland. Scott. J. Geol. *54*, 87–97.

10. Harris, J.P., and Hudson, J.D. (1980). Lithostratigraphy of the Great Estuarine Group (Middle Jurassic), Inner Hebrides. Scott. J. Geol. *16*, 231–250.

11. dePolo, P.E., Brusatte, S.L., Challands, T.J., Foffa, D., Wilkinson, M., Clark, N.D.L., Hoad, J., Pereira, P.V.L., Ross, D.A., and Wade, T.J. (2020). Novel track morphotypes from new tracksites indicate increased Middle Jurassic dinosaur diversity on the Isle of Skye, Scotland. PLoS ONE *15*, e0229640.

12. Bennett, S.C. (1995). A statistical study of *Rhamphorhynchus* from the Solnhofen Limestone of Germany: year-classes of a single large species. J. Paleontol. *69*, 569–580.

13. Padian, K., and Lamm, E.L. (2013). Bone Histology of Fossil Tetrapods (University of California Press).

14. Castanet, J., Croci, S., Aujard, F., Perret, M., Cubo, J., and de Margerie, E. (2004). Lines of arrested growth in bone and age estimation in a small primate: Microcebus murinus. J. Zool. *263*, 31–39.

15. de Margerie, E., Cubo, J., and Castanet, J. (2002). Bone typology and growth rate: testing and quantifying 'Amprino's rule' in the mallard (*Anas platyrhynchos*). C. R. Biol. *325*, 221–230.

16. Prondvai, E., Stein, K., Ősi, A., and Sander, M.P. (2012). Life history of *Rhamphorhynchus* inferred from bone histology and the diversity of pterosaurian growth strategies. PLoS ONE *7*, e31392.

17. Wang, X., Kellner, A.W.A., Jiang, S., Cheng, X., Wang, Q., Ma, Y., Paidoula, Y., Rodrigues, T., Chen, H., Sayão, J.M., et al. (2017). Egg accumulation with 3D embryos provides insight into the life history of a pterosaur. Science *358*, 1197–1201.

18. Padian, K., Horner, J.R., and De Ricqlès, A. (2004). Growth in small dinosaurs and pterosaurs: the evolution of archosaurian growth strategies. J. Vertebr. Paleontol. *24*, 555–571.

19. Woodward, H.N., Freedman, E.A., Farlow, J.O., and Horner, J.R. (2015). *Maiasaura*, a model organism for extinct vertebrate population biology: a large sample statistical assessment of growth dynamics and survivorship. Paleobiology *41*, 503–527.

20. Venditti, C., Baker, J., Benton, M.J., Meade, A., and Humphries, S. (2020). 150 million years of sustained increase in pterosaur flight efficiency. Nature *587*, 83–86.

21. Hone, D., Ratcliffe, J.M., Riski, D.K., Hermanson, J.W., and Reisz, R.R. (2021). Unique near isometric ontogeny in the pterosaur *Rhamphorhynchus* suggests hatchlings could fly. Lethaia *54*, 106–112.

22. Wang, X., Kellner, A.W., Jiang, S., and Meng, X. (2009). An unusual long-tailed pterosaur with elongated neck from western Liaoning of China. An. Acad. Bras. Cienc. *81*, 793–812.

23. Wang, X., Jiang, S., Zhang, J., Cheng, X., Yu, X., Li, Y., Wei, G., and Wang, X. (2017). New evidence from China for the nature of the pterosaur evolutionary transition. Sci. Rep. *7*, 42763.

24. Codorniú, L., Paulina Carabajal, A., Pol, D., Unwin, D., and Rauhut, O.W. (2016). A Jurassic pterosaur from Patagonia and the origin of the pterodactyloid neurocranium. PeerJ *4*, e2311.

25. Andres, B., and Myers, T.S. (2012). Lone star pterosaurs. Earth Environ. Sci. Trans. R. Soc. Edinb. *103*, 383–398.

26. Andres, B., Clark, J., and Xu, X. (2014). The earliest pterodactyloid and the origin of the group. Curr. Biol. *24*, 1011–1016.

27. Britt, B.B., Dalla Vecchia, F.M., Chure, D.J., Engelmann, G.F., Whiting, M.F., and Scheetz, R.D. (2018). *Caelestiventus hanseni* gen. et sp. nov. extends the desert-dwelling pterosaur record back 65 million years. Nat. Ecol. Evol. *2*, 1386–1392.

28. Dalla Vecchia, F.M. (2009). Anatomy and systematics of the pterosaur *Carniadactylus* gen. n. rosenfeldi (Dalla Vecchia, 1995). Riv. Ital. Paleontol. Stratigr. *115*, 159–188.

29. Dalla Vecchia, F.M. (2019). *Seazzadactylus venieri* gen. et sp. nov., a new pterosaur (Diapsida: Pterosauria) from the Upper Triassic (Norian) of northeastern Italy. PeerJ *7*, e7363.

30. Kammerer, C.F., Nesbitt, S.J., Flynn, J.J., Ranivoharimanana, L., and Wyss, A.R. (2020). A tiny ornithodiran archosaur from the Triassic of Madagascar and the role of miniaturization in dinosaur and pterosaur ancestry. Proc. Natl. Acad. Sci. USA *117*, 17932–17936.

31. Kellner, A.W. (2003). Pterosaur phylogeny and comments on the evolutionary history of the group. Geol. Soc. Lond. Spec. Publ. *217*, 105–137.

32. Lü, J., and Ji, Q. (2006). Preliminary results of a phylogenetic analysis of the pterosaurs from western Liaoning and surrounding areas. J. Paleontol. Soc. Korea *22*, 239.

33. Unwin, D. (2003). On the phylogeny and evolutionary history of pterosaurs. Geol. Soc. Lond. Spec. Publ. *217*, 139–190.

34. Vidovic, S.U., and Martill, D.M. (2014). *Pterodactylus scolopaciceps* Meyer, 1860 (Pterosauria, Pterodactyloidea) from the Upper Jurassic of Bavaria, Germany: the problem of cryptic pterosaur taxa in early ontogeny. PLoS ONE *9*, e110646.

35. Vidovic, S.U. (2016). A discourse on pterosaur phylogeny (University of Portsmouth), PhD thesis.

36. Carpenter, K., Unwin, D., Cloward, K., and Miles, C. (2003). A new scaphognathine pterosaur from the Upper Jurassic Morrison Formation of Wyoming, USA. Geol. Soc. Lond. Spec. Publ. *217*, 45–54.

37. O'Sullivan, M., Martill, D.M., and Groocock, D. (2013). A pterosaur humerus and scapulocoracoid from the Jurassic Whitby Mudstone Formation, and the evolution of large body size in early pterosaurs. Proc. Geol. Assoc. *124*, 973–981.

38. Andres, B., Clark, J.M., and Xing, X. (2010). A new rhamphorhynchid pterosaur from the Upper Jurassic of Xinjiang, China, and the phylogenetic relationships of basal pterosaurs. J. Vertebr. Paleontol. *30*, 163–187.

39. O'Sullivan, M., and Martill, D.M. (2018). Pterosauria of the Great Oolite Group (Bathonian, Middle Jurassic) of Oxfordshire and Gloucestershire, England. Acta Palaeontol. Pol. *63*, 617–644.

40. Brusatte, S.L., O'Connor, J.K., and Jarvis, E.D. (2015). The origin and diversification of birds. Curr. Biol. *25*, R888–R898.

41. Benson, R.B.J., and Choiniere, J.N. (2013). Rates of dinosaur limb evolution provide evidence for exceptional radiation in Mesozoic birds. Proc. Biol. Sci. *280*, 20131780.

42. Sullivan, C., Yuan, W., Hone, D.W.E., Wang, Y., Xu, X., and Zhang, F. (2014). The vertebrates of the Jurassic Daohugou Biota of northeastern China. J. Vertebr. Paleontol. *34*, 243–280.

43. Butler, R.J., Benson, R.B., and Barrett, P.M. (2013). Pterosaur diversity: untangling the influence of sampling biases, Lagerstätten, and genuine biodiversity signals. Palaeogeogr. Palaeoclimatol. Palaeoecol. *372*, 78–87.

44. Dean, C.D., Mannion, P.D., and Butler, R.J. (2016). Preservational bias controls the fossil record of pterosaurs. Palaeontology *59*, 225–247.

45. Benson, R.B.J. (2018). Dinosaur macroevolution and macroecology. Annu. Rev. Earth Planet. Sci. *49*, 379–408.

46. Close, R.A., Friedman, M., Lloyd, G.T., and Benson, R.B. (2015). Evidence for a mid-Jurassic adaptive radiation in mammals. Curr. Biol. *25*, 2137–2142.

47. Prentice, K.C., Ruta, M., and Benton, M.J. (2011). Evolution of morphological disparity in pterosaurs. J. Syst. Palaeontology *9*, 337–353.

48. Vlassenbroeck, J. (2006). Octopus 8: a high performance tomographic reconstruction package for X-ray tube and synchrotron micro-CT. In Advances in X-ray Tomography for Geomaterials (Wiley), pp. 167–173.

49. Cullen, T.M., Evans, D.C., Ryan, M.J., Currie, P.J., and Kobayashi, Y. (2014). Osteohistological variation in growth marks and osteocyte lacunar density in a theropod dinosaur (Coelurosauria: Ornithomimidae). BMC Evol. Biol. *14*, 231.

50. Harris, J.P. (1992). Mid-Jurassic lagoonal delta systems in the Hebridean basins: thickness and facies distribution patterns of potential reservoir sandbodies. Geol. Soc. Lond. Spec. Publ. *62*, 111–144.

51. Morton, N., and Dietl, G. (1989). Age of the Garantiana Clay (Middle Jurassic) in the Hebrides Basin. Scott. J. Geol. *25*, 153–159.

52. Hudson, J.D., Clements, R.G., Riding, J.B., Wakefield, M.I., and Walton, W. (1995). Jurassic paleosalinities and brackish-water communities: a case study. Palaios *10*, 392–407.

53. Evans, S.E., and Kermack, K.A. (1997). Assemblages of small tetrapods from the Early Jurassic of Britain. In In the Shadow of the Dinosaurs: Early Mesozoic Tetrapods, N.C. Fraser, and H.D. Sues, eds. (Cambridge University Press), pp. 271–283.

54. Fraser, N.C., and Sues, H.D. (1997). In the Shadow of the Dinosaurs: Early Mesozoic Tetrapods (Cambridge University Press).

55. Vincent, A.J., and Tyson, R.V. (1999). Organic facies of the Middle Jurassic of the Inner Hebrides, Scotland. Petrol. Geosci. *5*, 83–92.

56. Hudson, J.D., and Andrews, J.E. (1987). The diagenesis of the Great Estuarine Group, Middle Jurassic, Inner Hebrides, Scotland. Geol. Soc. Lond. Spec. Publ. *36*, 259–276.

57. Hammer, Ø., Harper, D.A., and Ryan, P.D. (2001). PAST: paleontological statistics software package for education and data analysis. Palaeontol. Electronica *4*, 1–9.

Current Biology
Report

⌘ CellPress

STAR★METHODS

KEY RESOURCES TABLE

REAGENT or RESOURCE	SOURCE	IDENTIFIER
Software and algorithms		
Avizo 9.1	Thermo Fisher Scientific	https://www.thermofisher.com/br/en/home/industrial/electron-microscopy/electron-microscopy-instruments-workflow-solutions/3d-visualization-analysis-software/avizo-materials-science.html
Mimics	Materialise	https://www.materialise.com/en/medical/mimics-innovation-suite/mimics
Trainable Weka Segmentation	ImageJ	https://imagej.net/plugins/tws/
TNT	[46]	http://www.lillo.org.ar/phylogeny/tnt/

RESOURCE AVAILABILITY

Lead contact
Further information and requests for resources should be directed to and will be fulfilled by the lead researcher Natalia Jagielska (Natalia.Jagielska@ed.ac.uk) or project supervisor Stephen L. Brusatte (Stephen.Brusatte@ed.ac.uk)

Materials availability
The holotype specimen is stored in the National Museum of Scotland (Edinburgh, Scotland, UK) under the collection number NMS G.2021.6.1-4. This is a public repository where the specimen is permanently available for research.

Data and code availability

- Data are publicly available as of the date of publication. Accession numbers are listed here. The 3D μCT scan of the crania and cervicals can be accessed from the data repository MorphoSource 000420017; photogrammetric surface scan of the main slab (dorsum) is reposited in 000420101, 000420110; photogrammetric surface scan of the counterslab is available at 000420118, 000420126. The phylogenetic and wingspan analyses are included in the supplementary information and Data S1. The TNT matrix, measurements, segmented cranial/cervical elements are included in Data S1 and S2.
- This paper does not report original code.
- Any additional information required to reanalyze the data reported in this paper is available from the lead contact upon request.

EXPERIMENTAL MODEL AND SUBJECT DETAILS

The main subject of this study, the holotype specimen NMS G.2021.6.1-4, is a well preserved, articulated, and reasonably complete skeleton preserved in a lagoonal bioclastic limestone (Figures 1, 2, 3, S2, and S3). The exposed anterior skull of the specimen was discovered at Brothers' Point, Isle of Skye, Scotland, by AP during a National Geographic-funded fieldtrip led by SLB on May 23, 2017 (Figure S1). The entire specimen was recovered by the team (including SLB, TJC, AP, DAR, and NDLC) on May 24-25, 2017. The brunt of collection work was conducted by DAR using a diamond-tipped rock saw. All fieldwork was conducted under a permit from Scottish Natural Heritage. The skeleton was found in the Upper Lonfearn Member of the Lealt Shale Formation (Great Estuarine Group), at a site that is referred to as Brothers' Point (BP) 3 in the literature.[11] BP3 is located immediately west of the mouth of Lonfearn Burn into Port Earlish (57.5863°N, 6.1494°W).

Comparative data on other specimens/taxa was retrieved from personal observations and the literature.

METHOD DETAILS

Fossil genuineness
As our team discovered the specimen *in situ*, we can confirm its genuineness. The specimen was mechanically prepared by Nigel Larkin, which involved gluing broken bones together and removing limestone matrix to expose the bones, but no other modifications. During collection and preparation, the fossil was separated into four slabs. The largest slab—what we refer to in the text as the 'main slab'—contains the greatest number of bones (trunk, forelimbs, sacrum and tail bones) exposed in dorsal view. The second

slab—what we refer to in the text as the 'main counterslab'—includes partial trunk, tail, pelvic and hindlimb, and left forelimb elements exposed in ventral view (the underside of the slab also contains the second wing phalanx). The third slab contains the third wing phalanx with an articulation point. The fourth slab includes the skull and anterior cervical vertebrae, exposed in dorsal view. The first and second slabs were separated from each other by hammer and chisel during the removal of the skeleton from the field site. The third slab was also separated from the remainder of the skeleton during field excavation. The fourth slab was removed from the first slab by Nigel Larkin during preparation, so that it could be μCT scanned.

Fossil examination
NMS G.2021.6.1-4 was studied first-hand in the University of Edinburgh Deep Time palaeontology laboratory by many of the authors, principally NJ and SLB. The specimen was photographed by GFF and NJ using a Nikon D850 camera with Nikkor 14-24 mm and MicroNikkor 60 mm lenses. Where adjustments were made to contrast, brightness, or white balance, they were applied to the whole image. After image adjustment, the background was digitally removed. Some images were created using the automated focus-stacking mode of the Nikon D850 to create enhanced-focus images in HeliconFocus v 7.5.5.

Computed tomography scanning
The skull and associated proximal cervical vertebrae were separated from the main slab by Nigel Larkin during preparation. The skull piece was then scanned using a custom-built X-ray μCT instrument at the School of GeoSciences, University of Edinburgh. Multiple, overlapping scans of the skull were acquired at 110 keV,and 50 W target power loading with a 0.9 mm copper and 1 mm aluminum energy filter, using 2 × 2 s exposure per projection (two frames averaged) and 2000 projections per scan. The scans were reconstructed by filtered back projection using Octopus v8.9 software.[48] The geometric voxel resolution of the scans was 97μm. The overlapping scans were registered and merged into a single volume using Avizo (version 9.1) and segmented manually in Mimics (Materialize N.V. 2014). Attempts were made for machine learning segmentation using the Trainable Weka Segmentation extension on Fiji/ImageJ, but with low contrast between bone and matrix and the presence of pyrite, manual segmentation in Mimics was required. While the μCT scan offered good contrast in regions where the ratio of matrix to bone is low, contrast was reduced in the posterior part of the skull (jugal, postorbital, squamosal), and manual segmentation of this region was challenging. These segmented regions are more interpretive and low-detailed (Figure 2). Although the posterior skull has reduced contrast and resolution, the internal spaces of the brain and ear region are well defined, making it possible to produce 3D endocasts. The dorsal section of the endocast is missing due to recent beach erosion, and the terminal region anteriorly is difficult to assess as the endocast opens to the vacuity around the orbits. The semi-circular canals can be segmented in part but are of too poor resolution to segment completely.

Bone histology
Thin sections (Figure S3) were prepared using a modified version of the method outlined by Padian and Lamm.[13] A portion of the wing phalanx was removed at a natural break, and was embedded in Buelher Epothin II epoxy resin under a vacuum (−1 atm). The epoxy was left to cure at room temperature for 48 h and was then cut at the target plane using a Buehler Isomet 1000 Precision Saw and a diamond-tipped wafering blade. The billet and an acrylic slide were each frosted on a glass plate using 600-grit silicon carbide abrasive slurry (Kemet International) to remove saw marks and increase surface area for adhesion. The billet was mounted to the slide using cyanoacrylate adhesive (Loctite) and was left to cure at room temperature for 3 h. The mounted billet was resectioned to 700 μm in thickness using the Buehler Isomet 1000 Precision Saw. The section was then polished by hand on a glass plate using 600-grit silicon carbide abrasive slurry (Kemet International) until optimal contrast was achieved. The slide was finished by polishing using a 1200-grit silicon carbide abrasive slurry (Kemet International) on a glass plate, and then two 10,000-grit lapping pads (Kemet International), the second of which was impregnated with mineral oil (Johnson & Johnson) to improve optical contrast. The slide was observed and photographed using a Leica DMLP Transmitted Light Polarizing Microscope and Leica Application Suite 4. Photomontages were created using the automated 'photomerge' tool in Photoshop Creative Cloud v22.4.1. Osteocyte lacunar density was calculated using the method of Cullen et al.[49]

Wingspan estimates
In order to estimate the wingspan of NMS G.2021.6.1-4 and isolated Taynton Limestone specimens, we utilized regression equations that predict wingspan based on the dimensions of single bones. These equations were constructed using data from two genera of basal pterosaurs (non-monofenestratan species closely related to *Dearc*) known from large samples that span a range of body sizes and ontogenetic stages: *Rhamphorhynchus* and *Dorygnathus*. We compiled measurement data for specimens of these genera for which both total wingspan and the lengths of the individual bones in question can be measured. Then, for each bone, we ran a separate regression equation: one using *Rhamphorhynchus* data only, the other using *Dorygnathus* data only.

All regressions were ordinary least-squares (OLS) regressions, performed in PAST, on log-transformed data. The source data for each regression, the resulting regression equations, regression plots (with 95% confidence intervals), and wingspan estimates for Dearc and isolated Taynton bones are provided in Data S1C–S1Q. Further explanation is given here:

Postcranial Bones
In order to estimate the wingspan of NMS G.2021.6.1-4 and Taynton Limestone pterosaurs, we carried out regression analyses using datasets consisting of the lengths of complete individual elements (humeri, ulnae, wing phalanges, and femora) and their corresponding complete wingspans. The humeral data were previously published in Appendix 1 of O'Sullivan et al.[37] Each one of the Jurassic

Current Biology
Report

CellPress

non-monofenestratan pterosaur specimens selected has at least one complete wing, which allows us to accurately measure the absolute wingspan. (Wingspan is defined as the length of one wing doubled. The body is not included as pterosaurs flew with the humerus and radius/ulna complex held in a v shape, the width of which is approximately equal to the lateral width of the body). We performed a total of 12 postcranial regressions: humerus, ulna, wing phalanx 1, wing phalanx 2, wing phalanx 4, and femur, in each case for *Rhamphorhynchus* and *Dorygnathus* separately. In each regression, we plotted the logarithms of wingspans along the y axis against the logarithms of lengths of a complete postcranial element (e.g., humerus, wing phalanx 1, etc.) on the x axis. For each regression, we then produced a line of best fit using OLS (with 95% CIs) and measured the variance of the data using the R^2 score and the significance of the linear relationship with a permutation p value. We then took the Linear Regression Equation from our plots and used it to estimate wingspan using the formula below.

$$\text{Wingspan} = m(\text{element length}) + b$$

Skull

We utilized the same regression methodology to use the skull length to estimate wingspan, but using only *Rhamphorhynchus*, as too few complete skulls of *Dorygnathus* are available to conduct a robust regression analysis.

Finally, we used our postcranial and cranial regressions to estimate the wingspan of two close relatives of *Dearc*: *Sericipterus* and *Angustinaripterus*. They have been described as large Jurassic pterosaurs, but their wingspans were estimated previously at 1.6-1.7 m based on fragmentary fossils and without explicit regression equations.

Stratigraphy, dating, and taphonomy

The Lealt Shale Formation (Figure S1) is Middle Jurassic in age. It is part of a package of formations known collectively as the Great Estuarine Group, which were formed during repeated cycles of delta progradation and retrogradation into marginally marine lagoonal systems between ca. 166-170 million years ago.[9] The dating of these rocks has historically been challenging because they do not preserve ammonites—the most relevant index fossils—in abundance.[9,50] However, their stratigraphic relationships with the underlying Bajocian Garantiana Clay Member and Bearreraig Sandstone Formation and the overlying Callovian Staffin Bay Formation constrain the age range for the Great Estuarine Group—and hence the Lealt Shale—to latest Bajocian to Bathonian.[50–53] The dating of the Lealt Shale in particular has been considered Bathonian, based on correlation with neighboring formations and the presence of ostracods in the overlying Duntulm Formation, which bear similarities to those of the *progracilis* zone.[9,10] If accurate, this would mean the Lealt Shale is coeval with the pterosaur-rich Taynton Limestone of England.

During the Bajocian-Bathonian, Britain was covered by a shallow epicontinental sea and divided into three major landmasses: London-Ardennes, Cornish-Mendip, and the northern Scottish-Pennine; the latter of which was where the Lealt Shale and other Skye deposits formed.[51] Around the end of the Bajocian, the offshore Hebridean Basin experienced sea-level rise, and became linked to neighboring basins by flooding of low grounds, which formed shallow areas of deposition with fluctuating salinity levels.[52] These events are represented by the lagoonal/marginal marine Lealt Shale and the deltaic Valtos formations of the Great Estuarine Group, both of which are well exposed on Skye. Much of the Hebridean Basin was very shallow at this time, and submerged areas closer to shore underwent periodic drying and subaerial exposure (as evidenced by terrestrial units with dessication cracks and salt deposition)[11]. The local climate during this time was warm and humid.[54]

The Lealt Shale (referred to as *Estheria* or *Mytilus* Shale in earlier literature),[10] is defined by an abrupt lithographic change from coarse-to-pebbled sandstone at the base (underlying Elgol Sandstone Formation) to bituminous, silty shale. The upper boundary is more gradational, turning from fissile muds to silts (overlying Valtos Sandstone Formation). There are notable changes in index fossils, exemplified by the disappearance of *Cyzicus* clam shrimp, and appearance of *Neomiodon* bivalve shells.[51,52] The Lealt Shale is tentatively divided into two members defined by the presence and abundance of *Mylitus* shells. The base is formed of monotypic *Praemytilus strathairdensi* shell-beds. This unit (the Kildonnan Member) is best exposed on the Isle of Eigg, as a gray silt shale, with occasional beds of limestone, and at least two bone beds and a coarse sandstone interval. The second member—the Lonfearn—is predominately composed of shales with ostracods, gastropods and the index fossil *Cyzicus*.[10] The holotype of the new pterosaur *Dearc* comes from the Lonfearn member.

The Lonfearn member is composed of three distinctive facies.[9] The fissile mudstone facies have shell plasters, high (4.5% max.) total organic content[55] and lack bioturbation suggesting low water energy and low oxygen levels. The shell limestone facies is composed of monotaxa *Neomiodon* shell beds replaced with biosparite and displaying effects of winnowing,[56] with variable levels of compaction. The new pterosaur skeleton originates from the ferruginous oolitic limestone facies, predominately composed of ooids with ferroan dolomite coating, with local muddy interbedding, pervasive fibrous calcite veins, disarticulated and winnowed bivalve shells and ostracods valves, which are found within a layer below the pterosaur specimen.

The pterosaur comes from a bed infilling sauropod trackway on a laminated micrite. It is a well-sorted, bioclastic limestone.[11] The bioclastic elements are chiefly disarticulated *Neomiodon* shells with some ostracods and conchostracans, although none have been found in the immediate vicinity of the skeleton. There are desiccation cracks present on the bed, set in some distance from the fossil, suggesting localized, periodic drying up periods in a shallow-water setting.[9] The skeleton is remarkably well preserved, with delicate and hollow bones mostly uncrushed and preserved in three dimensions, and it shows no evidence of substantial fracture, compaction, or disarticulation, suggesting it was buried in a low-energy environment, which dePolo et al.[11] suggested as biologically active mudflats.

The rock matrix within which the pterosaur skeleton resides is rich in evenly distributed diagenetic cubic pyrite (up to 3 mm), which surrounds and in some cases (e.g., left metacarpal) extends into the fossil. The Lealt Shale Formation is intruded by numerous dolerite sills but the pterosaur skeleton has not been visibly altered by diagenesis related to magmatism and metamorphism.

Nomenclatural acts

This publication and the nomenclatural acts it contains have been registered in ZooBank under the following LSIDs: LSID urn:lsid:-zoobank.org:pub:8087A873-85C2-447C-9B9C-F01F15E3189D.

Phylogenetic analysis

The phylogenetic relationships of *Dearc sgiathanach* among pterosaurs were tested using an analysis of discrete anatomical characters in a parsimony framework. The analysis includes 53 in-group terminal taxa and five outgroup taxa, scored for 155 unordered and equally weighted characters (Data S1B); we do not order multistate characters, to avoid any assumptions of transformation sequence. Characters include those assembled from numerous published pterosaur phylogenies and novel characters that particularly relate to features that are well preserved in *Dearc* (e.g., palatal, endocast, and ceratobranchial characters 71-79). Assembled characters originate from first-authored studies of Andres;[25,26] Britt;[27] Dalla Vecchia;[28,29] Kammerer;[30] Kellner;[31] Lu;[32] Unwin;[33] Vidovic;[34,35] Wang[22] [details in Data S2]. Characters exhibiting strong ontogenetic variation were excluded. Our taxon sample was constructed to focus on basal non-monofenestratan pterosaurs (the grade into which *Dearc* falls) and to mostly exclude taxa known only from immature specimens, which along with ontogenetically highly variable characters can confound phylogenetic analysis. We also excluded some taxa known only from highly incomplete or very poorly preserved specimens. We do note that we have included some taxa that are known mostly, or exclusively, from non-adult material or have immature type specimens: most notably *Dearc* itself, but also Triassic taxa like *Eudimorphodon* and kin, and *Anurognathus*. We elected to include such taxa because of their potential phylogenetic importance (they anchor major clades or fill important gaps in the stratigraphic record) and because specimens, although immature, exhibit good preservation and are relatively complete.

Fundamentally, we acknowledge that our phylogenetic analysis relies on a series of methodological choices, and other authors may prefer alternatives. Our main goals were to focus on the relationships of non-pterodactyloids and to minimize false phylogenetic signals that could derive from immaturity and incompleteness of specimens—a long-standing problem with pterosaurs. One alternative to the latter problem is to score ontogenetic-dependent characters as missing data ('?') for species with unknown mature specimens. However, we prefer not to use this approach, because it can be challenging to recognize ontogenetic stages in pterosaurs due to the plasticity of various indicators of maturity (bone fusion and ossification, body size, histology). For instance, without our histological evidence, we would probably have considered the *Dearc* a mature (or near-mature) adult, not a still-growing juvenile or sub-adult. Given such uncertainty, we prefer the more straightforward approach of simply removing specimens/taxa known from what are clearly very immature specimens or which are highly incomplete.

We performed a maximum parsimony analysis in TNT. We began with a New Technology Search (RSS, CSS, Ratchet, Drift, Tree Fusion with default settings), in which the minimal length tree was identified 50 times. A most parsimonious tree length of 491 was found 362 times. These trees were then subjected to an additional round of TBR branch swapping, which found a total of 9000 most parsimonious trees (overflow) most parsimonious trees (consistency index = 0.440, retention index = 0.731). We used these trees to conduct a strict consensus in which 27 taxa were excluded *a posteriori*, in order to eliminate wildcard taxa and specimens with a suspected preponderance of juvenile morphological scores. Clade support was determined using Bremer and bootstrap values. The strict consensus recovered *Dearc* in a clade with *Angustinaripterus longicephalus* and *Sericipterus wucaiwanensis*; this clade is sister to *Rhamphorhynchus muenstri*.

Institutional abbreviations

BYU, Museum of Paleontology, Brigham Young University, Provo, USA; CM, Carnegie Museum of Natural History, Pittsburgh, Pennsylvania, USA; IVPP, Institute of Vertebrate Paleontology and Paleoanthropology; MCSNB, Museo Civico di Scienze Naturali di Bergamo, Bergamo (Italy); MTM, Hungarian Natural History Museum, Budapest, Hungary; NHMUK, the Natural History Museum, London, UK; NMS, National Museums Scotland, Edinburgh; OUM, Oxford University Museum of Natural History, Oxford, UK; PMOL, Paleontological Museum of Liaoning, Shenyang Normal University, Shenyang, China; SMNK Staatliches Museum für Naturkunde Karlsruhe, Karlsruhe, Germany; SHN, Paleo at Sociedade de Historia Natural, Torres Vedras, Portugal; SMNS, Staatliches Museum für Naturkunde Stuttgart, Stuttgart, Germany; SNHM, State Museum of Natural History in Brunswick, Saxony, Germany; TMP, Royal Tyrrell Museum of Palaeontology, Drumheller, AB, Canada; ZDM, Zigong Dinosaur Museum.

QUANTIFICATION AND STATISTICAL ANALYSIS

The statistical analysis was performed using PAST 2.17.[57]

Supplemental Information

A skeleton from the Middle Jurassic of Scotland

illuminates an earlier origin of large pterosaurs

Natalia Jagielska, Michael O'Sullivan, Gregory F. Funston, Ian B. Butler, Thomas J. Challands, Neil D.L. Clark, Nicholas C. Fraser, Amelia Penny, Dugald A. Ross, Mark Wilkinson, and Stephen L. Brusatte
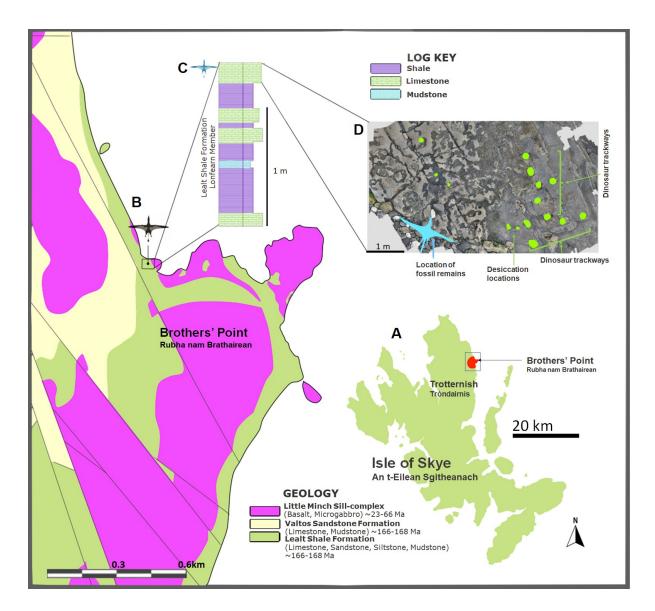
Figure S1. Locality information for the holotype of the new Middle Jurassic pterosaur *Dearc sgiathanach*, Related to STAR Methods. Map and geological context showing: Isle of Skye (a); geological map of the locality where the specimen was found, Brothers' Point (b); stratigraphic section at the discovery site (c); orthophoto of the pterosaur fossil location in relation to dinosaur trackways and evidence of desiccation (d). Figures c) & d) modified after dePolo et al. (2020).
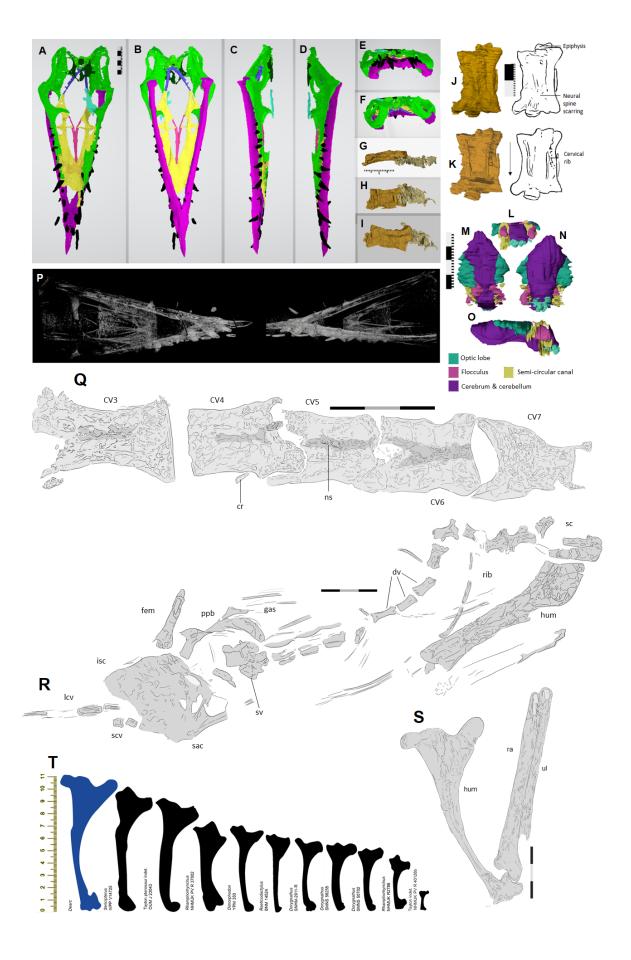
A B C D E F G H I J K L M N O

Epiphysis

Neural spine scarring

Cervical rib

Optic lobe
Flocculus
Semi-circular canal
Cerebrum & cerebellum

P

Q

CV3   CV4   CV5   CV7

cr   ns   CV6

sc

dv   rib

fem   ppb   gas   hum

isc

R   lcv

sv

scv

sac

S

ra

ul

hum

T

Deierc

Seriopterus
IVPP V14725

Tejton pterosaur indet.
OUM J 23043

Rhamphorhynchus
NHMUK PV R 37002

Dimorphodon
YPM 350

Raeticodactylus
BNM 14524

Dorygnathus
SMNS 2311-R

Dorygnathus
SMNS 56255

Dorygnathus
SMNS 50702

Rhamphorhynchus
NHMUK R62786

Tejton indet.
NHMUK PV R 4012fb

Figure S2. Skull and anterior cervical vertebrae of the new Middle Jurassic pterosaur *Dearc sgiathanach* **visualised by X-ray computed microtomography (manual & machine learning segmentation), Related to Figures 1-3.** Manually segmented skull in: (a) dorsal; (b) ventral; (c) right lateral; (d) left lateral; (e) anterior; (f) posterior views. Colour code: yellow – palate & pterygoid; purple – dentary; black – teeth; green – fused dorsal cranial elements; blue – basipterygoid; light blue – dorsal unfused cranial bones. Manually segmented atlas, axis & anterior cervical complex in: (g) lateral; (h) ventral; (i) dorsal views. Cervical close up with schematic line art in: (j) dorsal and (k) ventral views. Colour code: dark yellow – 3rd cervical; cream – atlas & axis. Manually segmented brain and inner ear endocast in: (l) anterior; (m) dorsal; (n) ventral; (o) left lateral views. Colour code [annotated in the figure] channels; dark blue – optic lobes; pink – flocculus; purple – cerebrum & cerebellum; light blue – cranial nerves; WEKA trained machine learning segmentation results (p) in dorsal and ventral (left to right, respectively). Line art of select elements (q) cervical vertebral series in dorsal view, abbreviations: cv# - cervical vertebra; cr - cervical ribs; ns - neural spine; NMS G.2021.6.3 counterslab (r) in ventral orientation, abbreviations: lcv - long caudal vertebra; scv - short caudal vertebra; isc - ischium; ppb - prepubis; sv - sacral vertebra (?); gas - gastralia; sac - sacrum; dv - dorsal vertebra; rib - dorsal ribs; hum - humerus; sc - scapula coracoid; and dorsal view of right humerus (s); abbreviations: hum - humerus; ra - radius; ul - ulna. Comparative size diagram of select non-pterodactyloid humeri (t) [annotated in image]. Scales bars=20 m
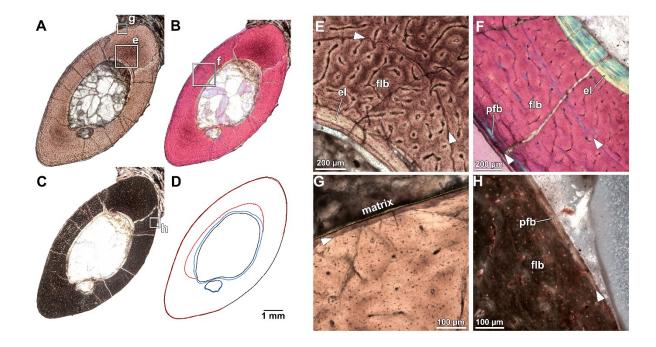
Figure S3. Histology of the wing phalanx of the new Middle Jurassic pterosaur *Dearc sgiathanach*, Related to STAR Methods. Thin section in plane polarized light (a), cross-polarized light with a lambda filter (b), cross-polarized light (c), and illustration (d) of histological features: lines of arrested growth (red) and endosteal resorption (blue). Note position of external line of arrested growth very close to the external surface. (e) Inner cortex of wing phalanx under plane polarized light, showing densely vascularized fibrolamellar bone with a line of arrested growth (arrows). (f) Cortex of wing phalanx under cross-polarized light with a lambda filter, showing endosteal lamellae (el), lines of arrested growth (arrows), predominance of primary fibrolamellar bone (flb), and an external zone of parallel-fibered bone (pfb). Note parallel-fibered bone (appearing cyan) adjacent to the line of arrested growth. (g) External cortex of wing phalanx under plane polarized light, showing line of arrested growth (arrow) adjacent to the external bone surface (below dotted yellow line). (h) External cortex of wing phalanx under cross-polarized light, showing parallel-fibered bone (pfb) at the periosteal surface, possibly indicating a decrease in growth rate from the earlier fibrolamellar bone (flb). Arrows denote lines of arrested growth. **Abbreviations**: **el**, endosteal lamellae; **flb**, fibrolamellar bone; **pfb**, parallel-fibered bone.
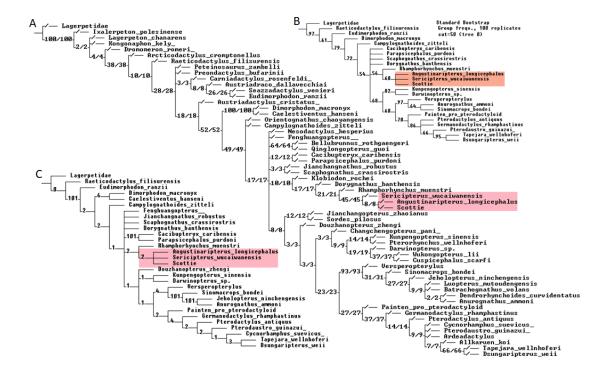
Figure S4. Results of phylogenetic analysis of the relationships of *Dearc sgiathanach* and other basal pterosaurs, Related to Figure 4 and STAR Methods. (a) Bootstrap Frequency difference (GC) tree without wildcard or problematic taxa removal from consensus (GC, 100 replicates); (b) Bootstrap absolute frequency tree with problematic taxa removed; (c) Bremer support values, (Bremer.run) with removal of problematic taxa. In each, the red box denotes the clade Angustinaripterini.

SUPPLEMENTAL REFERENCES

S1. Seeley H. G. (1870). The Ornithosauria: an elementary study of the bones of pterodactyles, made from fossil remains found in the Cambridge Upper Greensand, and arranged in the Woodwardian Museum of the University of Cambridge. Deighton, Bell.
S2. Plieninger, F. (1901). Beitrage zur Kenntnis der Flugsaurier. Palaeontographica 48, 65-90.
S3. Andres B., Clark J. M., & Xing X. (2010). A new rhamphorhynchid pterosaur from the Upper Jurassic of Xinjiang, China, and the phylogenetic relationships of basal pterosaurs. Journal of Vertebrate Paleontology, 30(1), 163-187.
S4. Andres B., Clark J., & Xu X. (2014). The earliest pterodactyloid and the origin of the group. Current Biology, 24(9), 1011-1016.
S5. He X. L., Yan D., Su D. (1983). A new pterosaur from the Middle Jurassic of Dashanpu, Zigong, Sichuan. Journal of Chengdu College of Geology, 1, 27-33.
S6. Eck K. E., Elgin R. A., Frey E. (2011). On the osteology of Tapejara wellnhoferi Kellner 1989 and the first occurrence of a multiple specimen assemblage from the Santana Formation, Araripe Basin, NE-Brazil. Swiss Journal of Palaeontology 130.2, 277.
S7. O'Sullivan M., Martill D.M. (2015). Evidence for the presence of Rhamphorhynchus (Pterosauria: Rhamphorhynchinae) in the Kimmeridge Clay of the UK. Proceedings of the Geologists' Association, 126(3), 390-401.
S8. Hübner M., Gischler E., Kosma R. (2020). Rare pterosaur remains tentatively referred to Dorygnathus banthensis (Theodori, 1830) from the Lower Jurassic (Posidonia Shale) of Schandelah (Lower Saxony, Germany). Braunschweiger Naturkundliche Schriften, Heft 16. 2020, 2020(16), 59-82.
S9. Wellnhofer P. (1975). Die Rhamphorhynchoidea (Pterosauria) der Oberjura-Plattenkalke Suddeutschlands. (Palaeontogr A, 148)
S10. Bennett S. C. (2014). A new specimen of the pterosaur Scaphognathus crassirostris, with comments on constraint of cervical vertebrae number in pterosaurs. Neues Jahrbuch für Geologie und Paläontologie-Abhandlungen, 327-348.
S11. Padian K. (2008). Early Jurassic pterosaur Dorygnathus banthensis (Theodori, 1830) and The Early Jurassic pterosaur Campylognathoides (Strand, 1928) Special Papers in Palaeontology (80).
S12. O'Sullivan M., Martill D. M. (2013). The taxonomy and systematics of Parapsicephalus purdoni (Reptilia: Pterosauria) from the Lower Jurassic Whitby Mudstone Formation, Whitby, UK. Historical Biology, 29(8), 1009-1018
S13. Owen R. (1859). On the vertebral characters of the order pterosauria, as exemplified in the genera Pterodactylus (Cuvier) and Dimorphodon (Owen). Philosophical Transactions of the Royal Society of London, 149, 161-169.
S14. Bennett S. C. (1996). Year-classes of pterosaurs from the Solnhofen Limestone of Germany: taxonomic and systematic implications. Journal of Vertebrate Paleontology, 16(3), 432-44 4.
S15. Ősi A., Prondvai E., Frey E. B. Pohl. (2010). New interpretation of the palate of pterosaurs. The Anatomical Record: Advances in Integrative Anatomy and Evolutionary Biology, 293(2), 243-258.
S16. Gasparini Z., Fernández M., Fuente M. D. L (2004). A new pterosaur from the Jurassic of Cuba. Palaeontology, 47(4), 919-927.
S17. Witmer L.M., Chatterjee S., Franzosa J., & Rowe T. (2003). Neuroanatomy of flying reptiles and implications for flight, posture and behaviour. Nature, 425(6961), 950-953

S18. Bennett S. C. (1995). A statistical study of Rhamphorhynchus from the Solnhofen Limestone of Germany: year-classes of a single large species. Journal of Paleontology, 69(3) p. 569-580.

S19. Zhou C.F. (2014). Cranial morphology of a Scaphognathus-like pterosaur, Jianchangnathus robustus, based on a new fossil from the Tiaojishan Formation of western Liaoning, China. Journal of Vertebrate Paleontology, 34(3), 597-605.

S20. O'Sullivan M., Martill D. M (2018). Pterosauria of the Great Oolite Group (Bathonian, Middle Jurassic) of Oxfordshire and Gloucestershire, England. Acta Palaeontologica Polonica, 63(4).

S21. Jiang, S., Li, Z., Cheng, X. and Wang, X., (2020). The first pterosaur basihyal, shedding light on the evolution and function of pterosaur hyoid apparatuses. PeerJ, 8, p.e8292.

S22. Howse S. C. B. (1986). On the cervical vertebrae of the Pterodactyloidea (Reptilia: Archosauria). Zoological Journal of the Linnean Society, 88(4), 307-328.

S23. Butler R. J., Barrett P. M., Gower D. J. (2009). Postcranial skeletal pneumaticity and air-sacs in the earliest pterosaurs. Biology Letters, 5(4), 557-560.

S24. Wang X., Jiang S., Zhang J., Cheng X., Yu X., Li Y., Wei G., & Wang X. (2017). New evidence from China for the nature of the pterosaur evolutionary transition. Scientific Reports 7, no. 1, 1-9.

S25. Lü, J., Unwin D.M., Jin X., Liu Y., Ji Q. (2010). Evidence for modular evolution in a long-tailed pterosaur with a pterodactyloid skull. Proceedings of the Royal Society B: Biological Sciences, 277(1680), 383-389.

S26. Witton M. P. (2015). Were early pterosaurs inept terrestrial locomotors?. PeerJ, 3, e1018.

S27. Cobb S. E & Sellers W. I. (2020). Inferring lifestyle for Aves and Theropoda: a model based on curvatures of extant avian ungual bones. Plos one, 15(2), e0211173.

S28. Francillon-Vieillot H., Arntzen J. W. & Géraudie J. (1990). Age, growth and longevity of sympatric Triturus cristatus, T. marmoratus and their hybrids (Amphibia, Urodela): a skeletochronological comparison. Journal of Herpetology, 13-22.

S29. De Margerie E., Cubo J., Castanet J. (2002) Bone typology and growth rate: testing and quantifying 'Amprino's rule' in the mallard (Anas platyrhynchos). Comptes Rendues Biologies 325, 221–330.

S30. Lee A. H., Werning S. (2008). Sexual maturity in growing dinosaurs does not fit reptilian growth models. Proceedings of the National Academy of Sciences (USA) 105, 582-587.

S31. Prondvai E., Stein K., Ősi A. & Sander M. P. (2012). Life history of Rhamphorhynchus inferred from bone histology and the diversity of pterosaurian growth strategies. PLoS One, 7(2), e31392.

S32. Calderón T., DeMiguel D., Arnold W., Stalder G., Köhler M. (2019). Calibration of life history traits with epiphyseal closure, dental eruption and bone histology in captive and wild red deer. Journal of Anatomy 235, 205–216.

S33. Hone D., Ratcliffe J. M., Riski D. K., Hermanson J. W. & Reisz R. R. (2021). Unique near isometric ontogeny in the pterosaur Rhamphorhynchus suggests hatchlings could fly. Lethaia 54, 106-112.

S34. Naish D., Witton M. P., Martin-Silverstone E. (2021). Powered flight in hatchling pterosaurs: evidence from wing form and bone strength. Scientific Reports, 11(1), 1-15.

S35. Padian K., Horner J. R., and De Ricqlès A. (2004). "Growth in small dinosaurs and pterosaurs: the evolution of archosaurian growth strategies." Journal of Vertebrate Paleontology 24, no. 3, 555-571.

S36. Gross, W. (1934). Die Typen des mikroskopischen Knochenbaues bei fossilen Stegocephalen und Reptilien. Z Anat 103, 731–764.

S37. Steel, L. (2008). The palaeohistology of pterosaur bone: an overview. Zitteliana, Series B, 28, 109–125.

S38. Steel L. (2003). The John Quekett sections and the earliest pterosaur histological studies. Geological Society, London, Special Publications 217, no. 1, 325-334.

S39. Erickson G.M, Rauhut O, Zhonghe Z., Turner A. H., Inouye B. D. (2009). Was dinosaurian physiology inherited by birds? Reconciling slow growth in Archaeopteryx. PLoS ONE 4(10), e7390.

S40. Sayão J, M. (2003). Histovariability in bones of two pterodactyloid pterosaurs from the Santana Formation, Araripe Basin, Brazil: preliminary results. Geological Society of London, Special Publications 217, 335-342.

S41. de Ricqlès A., Padian K., Horner J. R., Francillon-Viello, H. (2000). Paleohistology of the bones of pterosaurs (Reptilia: Archosauria): anatomy, ontogeny, and biochemical implications. Zool J Linn Soc 129, 349–385.

S42. Bertozzo F., Da Silva B. C., Martill D., Marlene E. (2021). A large pterosaur femur from the Kimmeridgian, Upper Jurassic of Lusitanian Basin, Portugal. Acta Palaeontologica Polonica, 66

S43. Wang X., Kellner A.W., Jiang S., Cheng X., Wang Q., Ma Y., & Zhou Z. (2017). Egg accumulation with 3D embryos provides insight into the life history of a pterosaur. Science, 358(6367), 1197-1201.